

Morphology control in Ni/Ti multilayer neutron mirrors by ion-assisted interface engineering and B₄C incorporation

FREDRIK ERIKSSON,^{1,*}  NAUREEN GHAFOOR,¹ SJOERD BROEKHUIJSEN,¹ GRZEGORZ GRECZYNSKI,¹ NORBERT SCHELL,² AND JENS BIRCH¹

¹Thin Film Physics Division, Department of Physics, Chemistry and Biology (IFM), Linköping University, SE-581 83 Linköping, Sweden

²Helmholtz-Zentrum Geesthacht, Centre for Materials and Coastal Research, Institute for Materials Research, Max-Planck-Straße 1, 21502 Geesthacht, Germany

*fredrik.eriksson@liu.se

Abstract: The optical contrast and minimum layer thickness of Ni/Ti broadband neutron multilayer supermirrors is usually hampered by an interface width, typically 0.7 nm, caused by nanocrystallites, interdiffusion, and/or intermixing. We explore the elimination of nanocrystallites in combination with interface smoothening by modulation of ion assistance during magnetron sputter deposition of 0.8 to 6.4 nm thick Ni and Ti layers. The amorphization is achieved through incorporation of natural B₄C where B and C preferably bond to Ti. A two-stage substrate bias was applied to each layer; -30 V for the initial 1 nm followed by -100 V for the remaining part, generating multilayer mirrors with interface widths of 0.40–0.45 nm. The results predict that high performance supermirrors with m-values as high as 10 are feasible by using ¹¹B isotope-enriched B₄C combined with temporal control of the ion assistance.

Published by Optica Publishing Group under the terms of the [Creative Commons Attribution 4.0 License](#). Further distribution of this work must maintain attribution to the author(s) and the published article's title, journal citation, and DOI.

1. Introduction

Neutron scattering is a signal-limited technique, and neutron instrumentation is designed to compromise between intensity and resolution. Even though modern neutron sources provide ever higher fluxes, e.g., the European Spallation Source which will have the world's most powerful neutron source [1], the largest gain in neutron flux is expected to come from improving neutron optical components [2]. Multilayers with small periodicities and depth-graded supermirrors are the most important devices for neutron beam handling to increase utilization efficiency in neutron scattering experiments. Owing to the strong contrast in scattering length densities, Ni/Ti is the materials system of choice when developing reflective multilayer neutron optics for instrumentation such as monochromators, wave guides, and focusing devices [3,4].

The reflected absolute intensity as well as neutron energy range from state-of-the-art mirrors are hampered by a Ni/Ti interface width, typically 0.7 nm, caused by nanocrystallites, interdiffusion, and/or intermixing, limiting the optical contrast across the interface as well as limiting the minimum usable layer thickness in the mirror stack [5].

In metal multilayer structures with nanometer layers it is difficult to create abrupt interfaces because of kinetic roughening, interlayer diffusion, solid-state reactions at the interface, and crystallization. To overcome these problems different attempts have been made to improve the interface structure. For example, it has been possible to increase the reflectivity by the deposition of ultrathin Cr layers at the Ni/Ti interfaces [6], by reactive sputtering of the Ni layers in a mixed ambient of Ar and air [7,8], or O₂ [9], or N₂ [10], using NiC instead of pure Ni to reduce the

crystallite size [11], using a surfactant mediated growth [12], and by interface polishing using argon ion bombardment [13] in ion beam sputtering.

Nevertheless, state-of-the-art reflectivities remain significantly lower than theoretical predictions for Ni/Ti supermirrors. It can be noted that no attempts have been made to intentionally grow neutron multilayers in an amorphous state which would lead to smooth interfaces and reduced kinetic roughening. Such approach has only recently been presented for Cr/Sc multilayer X-ray mirrors with clear improvements on interfaces and layer conformity [14].

The first demonstration of a neutron supermirror was made using electron beam evaporation [15]. It is now well established however that in an evaporation process, due to a low energy of the evaporants, adatoms on the growing film surface do not have sufficient energy, leading to a kinetically limited growth with porous layers and interface roughness as a consequence. Instead, magnetron sputtering, where the energy of the adatoms is higher (~1-2 eV), allowing for a smoother two-dimensional growth, is generally used to realize these multilayers. Despite the fact that low-energy ions are inherently present in the plasma ambient during magnetron sputter deposition, these are rarely utilized to stimulate adatom mobility for this application. There are only a few reports mentioning the application of a substrate bias voltage to control the interaction between the growing multilayer and the plasma. A positive substrate bias voltage (10 - 65 V), repelling the ions in the plasma, has been applied to influence the growth kinetics and thereby the stress in magnetic Fe/Si supermirrors [16], a large negative bias voltage of -200 V has been applied, without motivation, during growth of Ni/Ti multilayers [17], and, although not magnetron sputtering, the influence of a bias voltage on the structure of Si/FeCo multilayers and crystallization of FeCo when using triode sputtering has been reported [18]. Bias voltages of +60 V to -400 V were found to increase the crystallinity, while the interface layer thickness remained the same. Thus, it can be concluded that to date no systematic study has been made using ion-assisted magnetron sputter deposition to improve the interface quality of multilayer neutron optics.

This study explores the possibility to introduce B and C into the Ni/Ti multilayer structure through B₄C co-deposition and to use a temporal control of the substrate bias voltage during growth to change the layer morphology and interface definition to improve the neutron reflectivity performance and allow thinner layers to be deposited. Based on the obtained results, predictions of supermirror performance is calculated for Ni/Ti multilayers containing low-neutron absorbing, isotope-enriched ¹¹B and C.

2. Experimental details

Multilayer thin films of Ni/Ti and B₄C-containing Ni/Ti have been deposited onto Si (100) substrates using ion-assisted DC magnetron sputter deposition. The 600-mm-diameter cylindrical deposition chamber is equipped with four 75-mm-diameter sputter sources tilted with an angle of 35° towards the substrate normal with a target-to-substrate distance of 150 mm. Between adjacent sputter sources high magnetic permeability μ-metal shielding is used to minimize cross contamination as well as to extend the magnetic field closer to the substrate. In front of the sputter sources fast-acting shutters allow for control of the sputtered flux and enables single layers, multilayers, as well as co-sputtered layers to be deposited.

The 10 × 10 × 0.5 mm³ substrates were rotating around the sample normal at constant rate of 7 rpm, directly in line of sight of all sputter sources. The substrate table was electrically isolated enabling a negative substrate bias voltage to be applied during growth. Although substrate heating was available depositions were performed at ambient growth temperatures (< 50 °C). The chamber was evacuated to a base pressure of 6.7 · 10⁻⁶ Pa (5 · 10⁻⁸ Torr) using a dual turbo molecular pump setup and was equipped with a loadlock to maintain a good vacuum and allow for easy sample exchange. The deposition system is described in more detail elsewhere [19].

Ultra-high purity argon gas (>99.99997%) was introduced to a working pressure of 3 mTorr (0.4 Pa), as measured with a capacitance manometer. Target discharges were established with power supplies in constant-power mode where discharge powers of 20 W and 60 W, as measured with closed shutters, were used for Ni (99.99%) and Ti (99.95%), respectively. This yielded Ni and Ti deposition rates of about 0.036 and 0.039 nm/s as determined from hard X-ray reflectivity measurements of single layer films. B₄C was continuously deposited during deposition the Ni/Ti multilayer structures by sputtering from a ^{nat}B₄C (99.5%) target using different discharge powers of 0, 17, 35, and 70 W.

Both single multilayer structures, with a period Λ of 10 nm and 5 repetitions, and stacked multilayer structures, with periods of $\Lambda = 1.6, 3.2, 6.4$, and 9.6 nm consisting of correspondingly 32, 16, 8 and 6 repetitions, in order to maintain about the same total thickness of each multilayer stack, were deposited. The nominal Ni and Ti layer thicknesses were kept equal, given a thickness ratio of $\Gamma = d_{Ni}/(d_{Ni} + d_{Ti}) = 0.5$, where d_{Ni} and d_{Ti} indicate the individual layer thicknesses. The single multilayer structures have been deposited with two different designs of ion assistance and with different amounts of B₄C-doping, while for the stacked multilayer structures only the B₄C-doping was varied. The layer thicknesses were not adjusted for the amount of incorporated B₄C at different B₄C target powers and thus the multilayer period increase the more B₄C that is included.

Either a constant substrate bias voltage of -30 V was applied, or a two-stage modulated substrate bias was employed, where the initial 1 nm of each layer was grown with -30 V substrate bias, followed by -100 V bias for the remaining part of the layer. The latter ion assistance design has proven successful in reducing roughness and eliminating interface mixing in multilayer X-ray mirrors [20,21].

The deposition system is mounted on a ultra-high load hexapod with high resolution 6-axis positioning at the High Energy Materials Science P07 beamline at PETRA III [5]. This allows for fine alignment of the sample with respect to the synchrotron X-ray beam enabling time-resolved X-ray diffraction data to be acquired during film growth. In situ wide angle X-ray scattering (WAXS) was performed in transmission mode geometry using a 200 μm high × 700 μm wide X-ray beam at 78 keV, and the diffracted X-rays were collected on a two-dimensional Perkin-Elmer detector at a distance of 2.1 m from the sample. Each image was acquired for 160 s, corresponding to ~20 turns of full 360° sample revolution, and each image thus includes diffraction information from a 3D volume of reciprocal space.

X-ray reflectivity measurements were performed on a Panalytical Empyrean diffractometer using a Cu X-ray tube, a parallel beam mirror with a 1/32° divergence slit on the primary side, and a parallel plate collimator and a collimator slit (0.27°) on the secondary side, together with a PIXcel detector in 0D mode. Reflectivity of single B₄C-containing Ni/Ti multilayers were measured in the range 0°-10° 2θ with a step size of 0.01°/step and a collection time of 1.75 s/step, giving a total measurement time of ~30 minutes.

Reflectivity simulations were performed using the GenX software. The optical constants of the materials were determined using tabulated scattering lengths and composition obtained by ERDA. In all simulations the densities of the layers were however fitted to the critical angle. In the simulations a Gaussian interface broadening, the same for each interface, was included to account for interface roughness and intermixing.

Elemental composition was determined for the samples grown with a constant substrate bias voltage using time-of-flight energy elastic recoil detection analysis (ToF-E ERDA) at the Tandem Laboratory at Uppsala University. A 34 MeV ¹²⁷I⁸⁺ primary beam having an incident angle of 67.5° relative to the surface normal was used, and the energy detector was placed at a recoil scattering angle of 45°. A detailed description of the experimental set-up has been given elsewhere [22,23]. The measured recoil ToF-E ERDA spectra were analyzed using the Potku

code [24] where the measured recoil energy spectrum of each element was converted to relative atomic concentrations with an accuracy of ± 0.5 at.%.

X-ray photoelectron spectroscopy (XPS) core-level spectra of B 1s, C 1s, Ni 2p and Ti 2p were acquired to analyze the chemical bonding structure of boron and carbon atoms within the layers using an Kratos Axis Ultra DLD spectrometer operating at a base pressure of 1.5×10^{-7} Pa (1.1×10^{-9} Torr) with monochromatic Al K α radiation. The spectra were acquired from a 0.3×0.7 mm 2 area centered at 3×3 mm 2 portion of the sample previously sputter-etched with 0.5 keV Ar ions incident at an angle of 70° from the surface normal.

In order to avoid uncertainties related to commonly used binding energy scale referencing against C 1s line of adventitious carbon [25] spectra were aligned to the Fermi level cut-off. Deconvolution and quantification were performed using the Casa XPS software based on measured peak areas and applying relative sensitivity factors supplied by the manufacturer [26].

An analytical Tecnai G2 UT FEG transmission electron microscope operating at 200 kV for a point-to-point resolution of 0.19 nm was used for transmission electron microscopy (TEM) studies. Microstructure and layer definition of Ni/Ti and B₄C-containing Ni/Ti multilayers were studied using both bright field and dark field imaging as well as high resolution cross-sectional TEM. Dark field imaging was used as an approach to effectively highlight crystalline regions in the sample, while high-resolution TEM was used to investigate the layered structure in the multilayers containing the thinnest periods. The cross-sectional samples were prepared using mechanical grinding and polishing followed by low-energy ion-beam milling using a Gatan precision ion polishing system.

Calculations of predicted neutron reflectivity performance has been carried out using the IMD software [27].

3. Results and discussion

3.1. Structure and morphology with and without B and C incorporation

Wide angle X-ray scattering measurements, performed immediately after growth, on the stacked multilayers are presented in Fig. 1. The detector size and distance from the sample allows diffraction from atomic plane distances >0.16 nm to be recorded using 78 keV photons. This corresponds to observing diffraction from the Ni (111) and (002), and Ti (110), (002), (101) and (102) atomic planes, if present. Most of the recorded diffraction spots, however, originate from the crystalline Si substrate and the Al₂O₃ sapphire viewing window, marked in Fig. 1 by circles and triangles, respectively.

In Fig. 1(a) the 2D X-ray diffraction pattern of a stacked Ni/Ti multilayer grown without B₄C and using a uniform ion assistance by applying a -30 V bias voltage is shown. Apart from substrate and window reflections, strong Ni 111 reflections are visible, showing that the layers under these conditions grow crystalline. There are also faint reflections that most probably correspond to a cubic Ni-Ti intermetallic, although this is not possible to conclusively determine. No other film reflections can be observed. Since the observed 111 film reflections appear as diffraction spots, rather than rings, with the strongest Ni 111 reflection in the growth direction, it can be concluded that the Ni layers are 111 textured, as commonly observed for an fcc metal due to minimization of the surface energies during growth. This is also consistent with other findings for Ni/Ti multilayers presented in the literature [28,29].

For growth under the same conditions, except for the addition of B₄C to the multilayer by co-sputtering (using a 35 W magnetron power), diffraction neither from Ni or any Ni-Ti is observed, as can be seen in the image in Fig. 1(b), and the multilayer is thus considered to be X-ray amorphous, meaning that any crystallites, if present, are too small to be detected using X-ray diffraction. In fact, any addition of B₄C, from the lowest to the highest applied B₄C magnetron power, causes the multilayers to become X-ray amorphous, irrespective of the used ion assistance design, as seen from the absence of the Ni 111 reflection in the region around

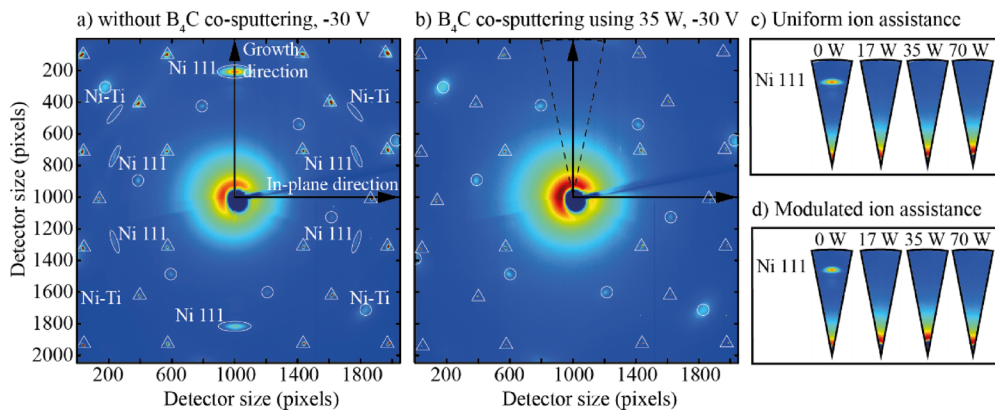


Fig. 1. Wide angle X-ray scattering a) without B_4C co-sputtering, -30 V b) B_4C co-sputtering using a magnetron power of 35 W, and c) influence of different B_4C powers on the Ni 111-formation in the growth direction. The open circles and triangles mark the diffraction spots of the Si substrate and the sapphire viewing window, respectively, while the open ellipses mark diffraction spots from Ni and Ni-Ti intermetallics.

the growth direction in Figs. 1(c) and (d). Without the addition of B_4C the Ni 111 reflection along the surface normal is present although more well-defined when using a modulated ion assistance, indicating a stronger 111 texture in this case. Although not clearly visible in the images in Fig. 1(c) and (d), multilayer reflections are present inside the Ni 111 diffraction spots along the growth direction, showing the presence of a multilayered structure perpendicular to the substrate normal, both for a uniform and a modulated ion assistance without B_4C co-sputtering. The reflections are however too few and diffuse to be used to accurately determine the multilayer periods in these stacked multilayers.

In Fig. 2 bright field TEM micrographs of single multilayer structures with a 10 nm periodicity and 5 repetitions are shown in two different length scales to provide both a close-up view and a larger overview of the structures. The crystalline layers with 111 faceted Ni crystallites, and diffuse contrast at the interfaces probably corresponding to Ni-Ti intermetallics at the interfaces (not detected in WAXS) are observed in Fig. 2(a) when no B_4C is added and a uniform ion assistance is used. Using B_4C co-sputtering and a constant ion assistance in b), the layers are amorphous but there is an accumulating roughness present showing that the applied substrate bias voltage results in insufficient adatom mobility leading to a kinetically limited growth. With B_4C co-sputtering and using a modulated substrate bias voltage, giving a higher ion energy bombardment in the end of each individual layer's deposition, shown in c), the layers are amorphous and smooth, and there is no significant accumulated roughness. The improved interface definition using a combination of B_4C co-sputtering and a modulated ion assistance is clearly shown in the overview micrographs in the top of Fig. 2.

From the wide-angle X-ray scattering measurements and TEM it was found that the multilayers were (X-ray) amorphous for all investigated B_4C concentrations. To investigate the influence of the amount of B_4C on the interface quality hard X-ray reflectivity (XRR) measurements and fitting were employed. In Fig. 3 XRR measurements are shown for periodic multilayers, similar to those presented in Figs. 2(b) and (c), grown with different ion assistance and increasing $B + C$ content. Since the position of the Bragg peaks are related to the period of the multilayer, the peak shifts towards smaller grazing incidence angles with increasing B_4C magnetron powers, shows that an increasing amount of B and C is being incorporated. For both a constant and a modulated ion assistance the periods increase linearly from about 9.7 nm to about 11.5 nm, i.e. by almost 19%, when increasing the B_4C magnetron power up to 70 W.

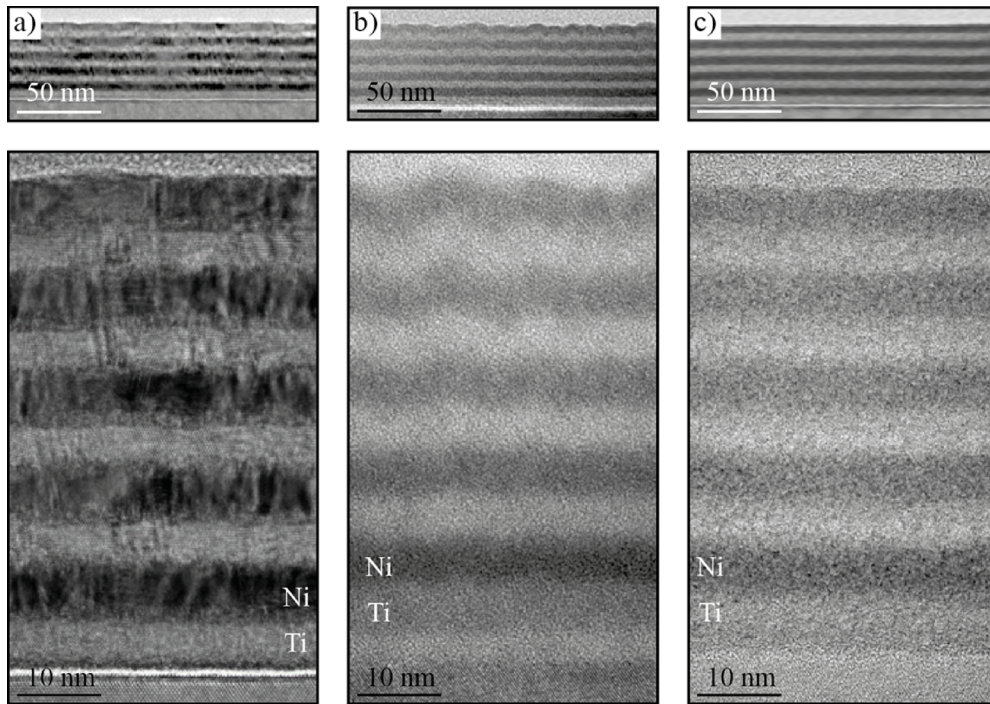


Fig. 2. Bright field TEM micrographs of single Ni/Ti multilayers showing the effect of ion assistance. In a) no B_4C is added and a constant ion assistance is applied during growth, while in b) 35 W B_4C co-sputtering is used with a constant ion assistance, and in c) 35 W B_4C co-sputtering and a modulated substrate bias voltage is applied. Overview micrographs are shown on top.

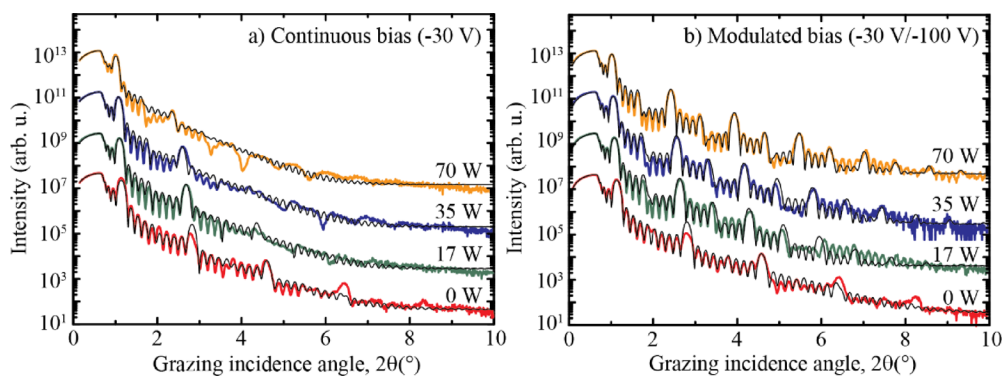


Fig. 3. X-ray reflectivity measurements of Ni/Ti multilayers ($\Lambda=10$ nm, $\Gamma=0.5$, $N=5$) grown using a) a constant ion assistance, and b) a modulated ion assistance, and increasing power of B_4C target. The measurements are vertically shifted for clarity and simulations are included as black solid lines.

Since the reflectivity profiles represent the Fourier transform of the electron density variation along the growth direction, more and sharper Bragg peaks qualitatively correspond to more well-defined interfaces that are more abrupt and flat. In addition, a regular appearance of closely spaced Kiessig fringes, in-between the Bragg peaks, is an evidence of a high layer thickness uniformity. When using B₄C co-sputtering and a constant ion assistance it can be seen from the reflectivity measurements in Fig. 3(a) that there are fewer Bragg peaks with lower intensities and more irregular Kiessig fringes when the amount of B and C in the multilayer is increased. Thus, even though the multilayers turn amorphous, as seen in TEM, the XRR shows that incorporation of B and C increasingly deteriorate the multilayer structure for increasing B₄C co-sputtering magnetron powers. This evolution is due to an effective reduction of the adatom mobility by formation of more metal-boron and metal-carbon bonds when increasing the amount of B and C atoms present in the multilayer, in combination with an insufficient kinetic adatom stimulus when using a continuous low energy ion assistance during growth by using a constant substrate bias voltage of -30 V.

When applying a modulated ion assistance with a higher ion energy in the end of each layer, Fig. 3(b), the resulting interface morphology evolution with increasing amount of B and C incorporation is completely different. Without addition of B and C (0 W B₄C magnetron power) the reflectivity profile is almost identical to the one when using a continuous ion assistance. However, with increasing B and C content the trend is now instead towards more Bragg peaks with higher intensities and more clear Kiessig fringes, indicating improved interface qualities with more B and C.

The low ion energy assistance during growth of the first 1 nm of each layer allows for the formation of an abrupt interface to each preceding layer thanks to little ion-induced intermixing. Although these initial parts of each layer are subject to roughening due to kinetically limited growth, the higher ion energy (~100 eV) in the remainder of each layer provides forward knock-on densification and an increasing adatom surface mobility forming a smooth top surface for the deposition of the next layer [20]. Thus, as seen from these results, when B₄C co-sputtering is used for layer amorphization, a modulated ion assistance is not only beneficial for the interface structure, but is in fact necessary for the formation of multilayers with high quality interfaces.

To confirm the qualitative observations made above, fittings were made to the measured reflectivity profiles to quantitatively determine the individual interface widths of Ni and Ti for the different growth conditions. As the XRR simulations inherently represent the concentration profile in the growth direction, the interface width represents the transition from one layer to the next averaged laterally along the interfaces. Although an accumulating roughness is evident from the transmission electron microscopy studies, the same interface width has been applied throughout the multilayer stack in the simulations, effectively resulting in an overestimated average interface width. The results are illustrated with the interface width as a function of the B + C content for a continuous ion assistance and a modulated ion assistance for Ni and Ti, respectively, in Fig. 4. As can be seen, the interface width is always smaller when using a modulated ion assistance, also without B and C incorporated in the multilayer. Within the error margins the interface width is about the same for both Ni and Ti, and it is not possible from these reflectivity fits to make any distinction if the B and C incorporation is particularly beneficial for one material over the other. The lowest simulated interface width is obtained for the multilayer grown using a modulated ion assistance and the highest amount of B and C incorporation. However, introducing more and more B and C into the multilayer structure will dilute the neutron optical contrast between the Ni and Ti layers, giving a lower reflectivity performance. Thus, there is a trade-off between a large amount of incorporated B and C and a reduced interface width to reach the highest possible neutron reflectivity. With this in consideration, we found that the optimum multilayers here are grown using a modulated ion assistance and a 35 W power to the B₄C magnetron. The reflectivity profile of this multilayer in Fig. 3(b) is also the one that have

the most clear Bragg peaks at the highest grazing incidence angles, and the reflectivity fitting yielded interface widths of about 0.45 nm as seen in Fig. 4. This is a significant improvement over current state-of-the-art Ni/Ti supermirrors which exhibit interface widths of 0.7 nm [5].

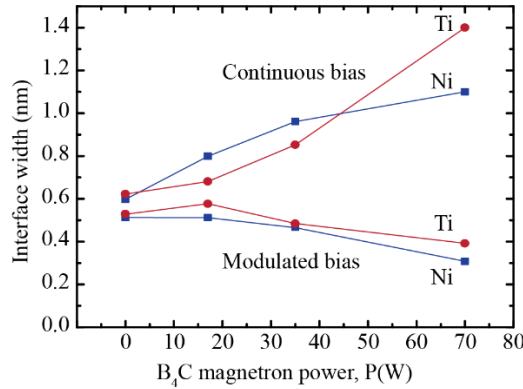


Fig. 4. Interface width evolution of Ni and Ti in Ni/Ti multilayers with increasing B₄C magnetron power, using either a continuous or a modulated ion assistance during growth.

3.2. Composition and chemical bonding with and without B and C incorporation

From the TEM micrographs in Fig. 2 it is clear that the incorporation of B and C into the multilayers has a significant effect on the microstructure. To determine the amount of incorporated B and C and the chemical bonding structure in the samples, ERDA and XPS analysis were performed, respectively.

The ERDA measurements have been performed on multilayer samples deposited using different B₄C magnetron powers with a continuous substrate bias of -30 V. The compositions of four multilayers are summarized in Table 1 where the values were extracted from the interior of the multilayer, i.e. ignoring the signal from the top surface and close to the substrate. A Ni-to-Ti ratio of 1.45 ± 0.05 is consistent for all samples, and it is clear that more B and C is being incorporated for higher magnetron powers and that these follow an almost linear relationship. The slight apparent deviation in B-to-C ratio falls within the precision of the measurement, which is <±0.5 at.%. The amount of H, O and N inside the multilayers is found to be negligible, i.e. < 0.5 at.%. It is suspected that the amount of B and C incorporation is not significantly affected by the applied ion assistance design as estimated by calculations of the sputtering yields using the SRIM software. In this manuscript it is chosen to use the sum of the boron and carbon content for representation.

Table 1. Multilayer composition as determined by ToF-ERDA.

P _{B4C} (W)	Ni (at.%)	Ti (at.%)	B (at.%)	C (at.%)	B/C	B + C (at.%)
0	58.0	40.6	1.1	0.3	-	1.4
17	52.5	34.7	10.0	2.8	3.6	12.8
35	46.2	32.9	16.2	4.7	3.4	20.9
70	38.4	26.3	28.4	7.0	4.1	35.4

For the XPS analysis the surface was first sputter-etched whereafter XPS depth profiling was performed for 20 minutes using a constant Ar⁺ ion energy of 0.5 keV at an incidence angle of 70° from the surface normal to a depth of about 90-120 Å from the surface, i.e. roughly corresponding to the thickness of one period at the top of the multilayer. The difference in the

total depths reached is because the sputtering rates during the depth profiling decreased with increasing amounts of B and C in the multilayers, from 6.5 Å/min without B₄C to 4.9 Å/min for samples deposited using 70 W B₄C, indicating the presence of a larger fraction of strong metal-boron and metal-carbon bonds that have higher surface binding energies than the pure elements.

In Fig. 5 the depth profiles are shown for multilayers grown without B₄C in a), and with B₄C using a magnetron power of 70 W in b), both using a modulated ion assistance. The observed signals from oxygen and carbon in the Ni and Ti layers in a) are likely a result of implantation and/or redeposition of these elements during sputter etching and depth profiling, the slight modulation with depth is likely due to the higher affinity of Ti for bonding with these elements. The same phenomenon is occurring in b) for O while eventual carbon impurities can not be discerned from carbon coming from the addition of B₄C.

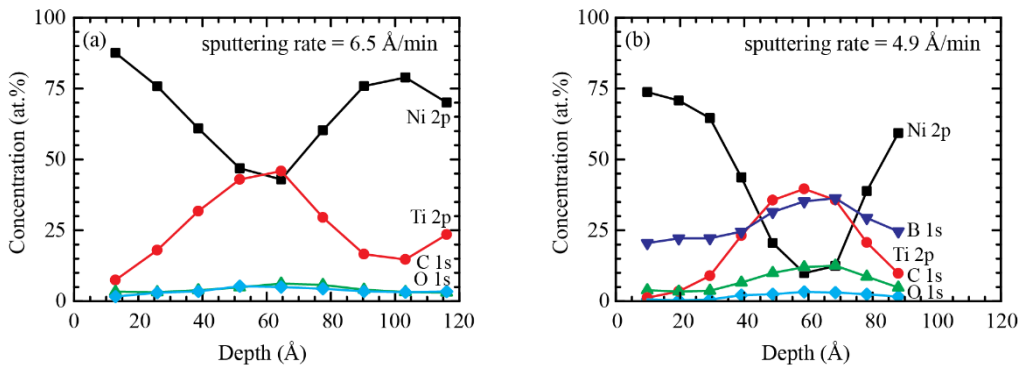


Fig. 5. XPS depth profiles showing the top layers of multilayers deposited without B₄C in (a), and with B₄C using a B₄C magnetron power of 70 W in (b).

The chemical modulation of Ni and Ti in both depth profiles shows that we indeed have multilayered structures, even though the concentration of Ni and Ti never reaches zero in the center of the layers. This is due to the limited depth resolution of XPS resulting from the fact that the probing depth, being in the range from 3 to 6 nm for Ti 2p and Ni 2p electrons in these materials [30] is comparable to the thickness of the individual layers used in this work. Thus, even at a depth corresponding to the center of one layer, a contribution from the underlying layer will be included in the signal. In addition, the interface mixing due to forward knock-on effects and surface roughening resulting from the sputter depth profiling prevents quantitative measures of the interface width. Nevertheless, important conclusions can be made from the depth profiles. The steeper slope of the compositional profile at the interface for the B₄C-containing multilayer in b) shows that the interfaces are better defined when adding B and C. In addition, it can be seen that the distribution of B and C is not uniform in the multilayer, instead both elements are preferentially located in the Ti layers, despite the deposition conditions being the same for both Ni and Ti. The sum of B and C reaches up to 50 at.% in the Ti layers while in the Ni layers it is only about half of that value. From ERDA we find that the sum of B and C gives an average of 35.4 at.% in the interior of the multilayer when deposited with 70 W B₄C. Such a compositional variation is, however, expected based on the calculated enthalpies of formation using the modified Miedema's model for Ti-B (-84 kJ/mol) and Ti-C (-77 kJ/mol) as compared to those for Ni-B (-33 kJ/mol) and Ni-C (+24 kJ/mol) [31], which indicate that B and C preferentially bond to Ti rather than Ni in order to minimize the total energy of the system. Another potential factor can be preferential resputtering of light B and C by the concurrent fluxes of Ar-ions and metal atoms during film growth. Since Ni is heavier than Ti one can expect a higher resputtering rate of light elements from the growing Ni layer surface due to a higher sputter yield amplification effect [32]

for Ar-ions and a higher momentum transfer from Ni. ERDA also shows how a thin oxide layer is formed on top of the pure sample, although the resolution is not sufficient to get an accurate assessment of the exact thickness. While there is some oxide formation of multilayers deposited with 17 W B₄C, there is no sign of oxidation for multilayers with higher amounts of B and C, showing that B₄C co-deposition effectively prevents surface oxidation.

Even though the compositional depth profiles of B and C seem to be correlated in the investigated range, the B-to-C ratio varies from 3 in the Ti layers to 6.5 in the Ni layers. Thus, even though the total amount of B and C is the highest in the Ti layers, the relative amount of B compared to C is lower. The average B/C ratio is 4.3 for the top multilayer period, which is comparable to the ratio of 4.1 that was found by ERDA when using a 70 W magnetron power for the B₄C target.

The B 1s, C 1s, Ni 2p, and Ti 2p high resolution spectra are plotted as a function of depth in Fig. 6 for samples with and without B and C addition. From the B 1s photoelectron spectra in Fig. 6(a) it is seen that the B 1s signal appears at 188.2 eV in the spectra dominated by the contribution from the Ni layer and shifts to 187.4 eV once the signal is recorded from the Ti layer. These binding energy values correspond to B-C and B-Ti bonds, respectively [33]. Hence, we can conclude that B bonds to C inside the Ni layers, and preferentially to Ti inside the Ti layers. This can again be explained in terms of the different enthalpies of formation for the different borides, given the binding enthalpy of B-C (-71 kJ/mol) [34]. The C 1s spectra shown in Figs. 6(b) and 6(c) confirm that C is bonding preferentially to B inside the Ni layers, and to Ti inside the Ti layer. It should be noted though that some residual C from the surface might have been implanted into the Ni and Ti layers to form Ni-C and Ti-C bonds due to the Ar ion etching during the sputter depth profiling.

To summarize the information from the binding energy shifts in XPS, B and C form stronger bonds with Ti than with Ni and preferentially resides inside the Ti layers.

3.3. Multilayer morphology for different periodicities

In Fig. 7 the cross-section of the stacked multilayers, corresponding to those discussed above in Fig. 1(a) and (b), are shown in bright field, dark field and high-resolution TEM micrographs. The nominal multilayer periods are indicated in the bright-field micrograph.

When studying the micrographs for the multilayer grown without B and C and using a uniform ion assistance in Fig. 7(a), it is seen for the larger multilayer periods of 6.4 and 9.4 nm that the interface roughness is correlated, i.e., replicated from layer to layer, and that it is increasing with thickness. Combined with the dark field micrograph in Fig. 7(b), obtained from the Ni 111 diffraction spot, the thicker layers clearly show a crystalline morphology and that the crystallite size is increasing in both laterally and vertically with increasing layer thickness, thus contributing to an interface roughness increase. Low density nanocolumnar voids interrupt the lateral growth and define a lateral roughness correlation length, and the strong Ni 111 texture results in faceted Ni crystallites causing the roughness in the growth direction. Low-density columnar voids typically form due to an insufficient lateral adatom mobility at room temperature growth conditions. TEM analysis of the two thicker periods also show that the Ti-on-Ni interface is rougher than the corresponding Ni-on-Ti interface. The asymmetric interface widths for Ni/Ti multilayers have previously been reported in the literature [35], and can arise due to the strong texture of the Ni layers.

The high-resolution micrograph in c) of the thinnest multilayer period close to the substrate shows that there are crystallites formed also in the thin layers. In addition, the high-resolution micrograph shows that there is no layered structure present when individual layers are 0.8 nm or less. The absence of a layered structure is due to a compositional intermixing of Ni and Ti forming disordered phases at low thicknesses [28].

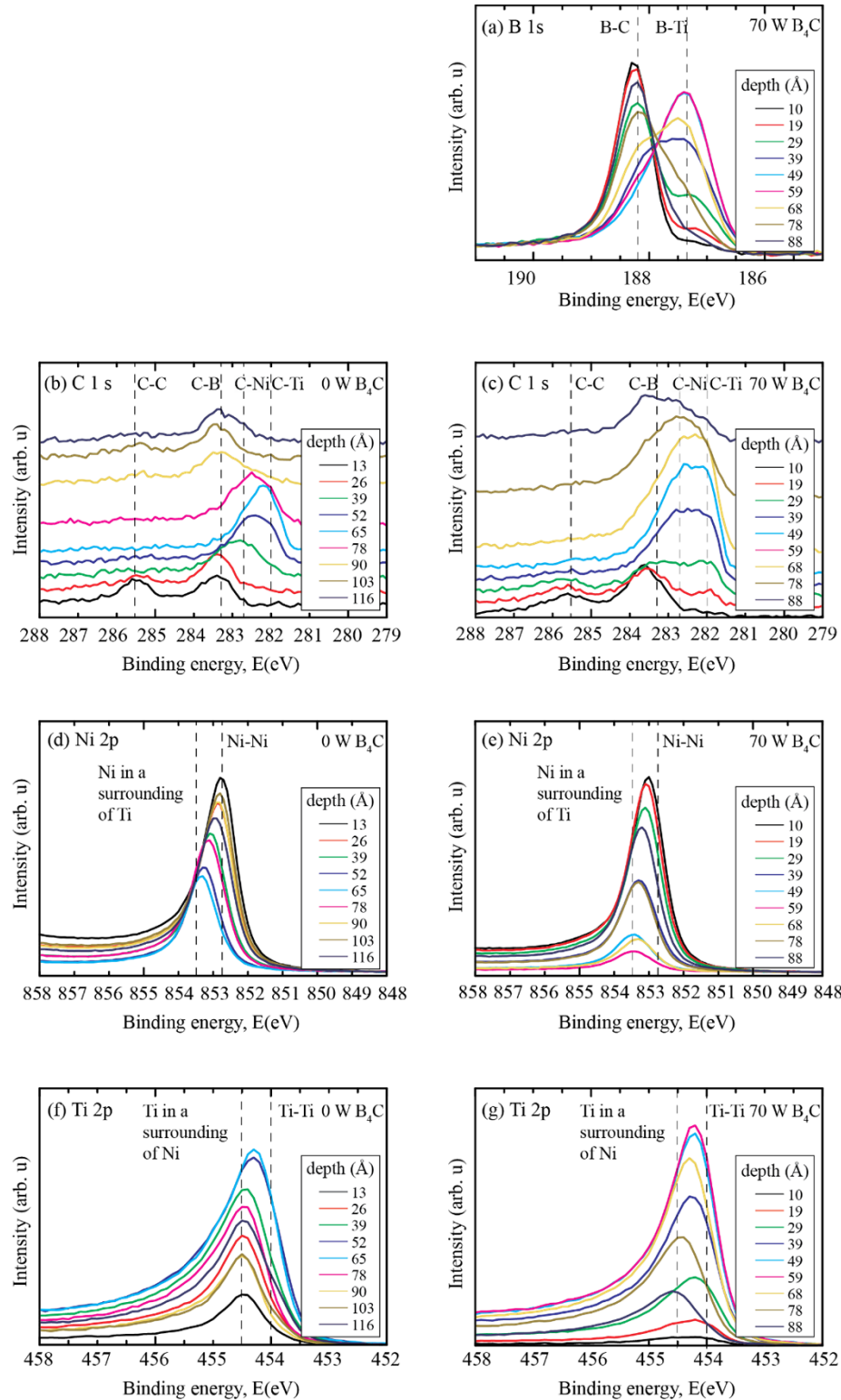


Fig. 6. X-ray photoelectron spectroscopy spectra of the B 1s, C 1s, Ni 2p and Ti 2p photoelectrons as a function of depth for the investigated Ni/Ti and B₄C-containing Ni/Ti multilayers.

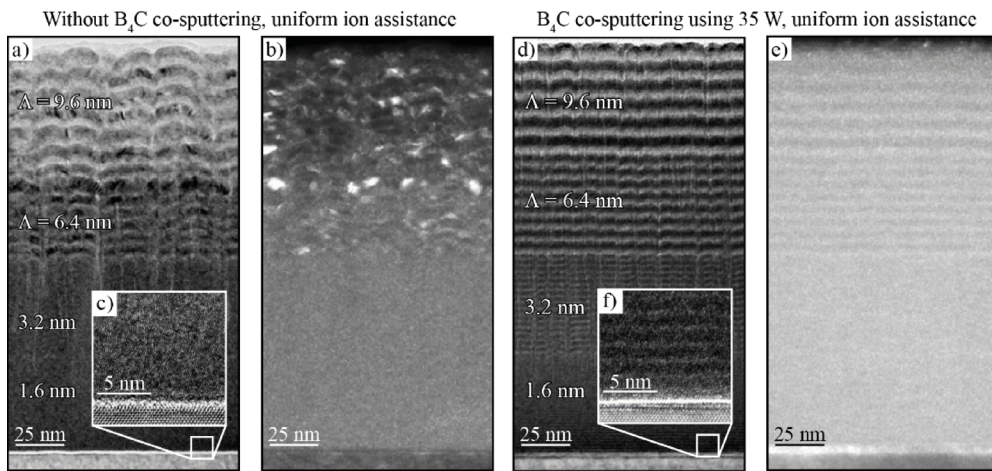


Fig. 7. Evolution of crystallinity in stacked Ni/Ti multilayers grown with and without B_4C co-sputtering and a constant ion assistance. a) Bright field micrograph, b) dark field micrograph, c) high-resolution micrograph of a Ni/Ti multilayer grown without B_4C . d) Bright field micrograph, e) dark field micrograph, and f) high-resolution micrograph of a Ni/Ti multilayer grown using 35 W B_4C co-sputtering.

The observations of crystalline layers, absence of periodicity in thin period multilayers, formation of interface intermetallics, and an accumulating interface roughness with total multilayer thickness, summarize very well the main features limiting the neutron reflectivity performance of Ni/Ti multilayers.

When introducing B and C into the Ni/Ti multilayer, Fig. 7(d), (e), and (f), the morphology changes significantly. Most obvious is the reduction of the interface roughness and accumulated roughness in d) and the complete absence of any crystallites in f). This indicates that B and C amorphize the Ni and Ti layers, independent of layer thicknesses, and that amorphous layers can be grown with minimum interface roughness. However, low density nanocolumnar voids, interrupting the lateral growth, extends all the way from the substrate to the top of the multilayer stack and give rise to a correlated interface roughness also when B and C is present. Combined with the analysis of the modulated ion assistance growth in Fig. 2(c), which indicates that B and C incorporation cause a roughness accumulation, and knowing that insufficient adatom mobility cause underdense layers, it is clear that the present deposition conditions are not sufficient to densify the layers. However, a high-flux modulated low-energy ion assistance scheme has proven to be a successful route to overcome these issues in Cr/Sc multilayers [14].

Finally, the high-resolution micrograph of the thinnest layers containing B and C in Fig. 7(f) confirm the formation of an amorphous layer structure throughout the multilayer stack but also that there is a clear chemical modulation visible for periods as short as 1.6 nm. This is in contrast to the pure Ni and Ti layers that mix into their disordered phases for thin layers. Thus, the incorporation of B and C provide a solution to hinder the intermixing and enable deposition of sub-nm thin layers.

3.4. Predicted neutron supermirror performance

Using the simulated interface widths the expected neutron reflectivity performance of B and C containing Ni/Ti multilayer mirrors can be predicted. Such predictions were carried out using the IMD software for depth-graded supermirrors where the layer thicknesses were equal for both Ni and Ti and varied from 2 nm at the substrate to 40 nm at the top following a power-law analytical depth-grading function, $z_j = 168.17/(j-0.97)^{0.25}$, where $j = 1$ at the top and reach

the total number of periods, $N = 5000$, at the substrate. Even though there exists more efficient algorithms for calculating the layer thickness distribution [36,37,38,39] this simple approach is sufficient to predict a supermirror performance. The thinnest layer in the multilayer stack determine the critical angle of the supermirror, and this layer design correspond to a supermirror with an m -value of 7.2. For the simulations a neutron wavelength of 0.3 nm was used.

Reflectivity calculations were performed for an ideal Ni/Ti supermirror without any interface width and for an interface width of 0.7 nm, which is state-of-the-art today [5], to compare to the predicted reflectivities for a B and C containing Ni/Ti supermirror. B and C concentrations of 16 at.% B and 4 at.% C were assumed in both the Ni and Ti layers, i.e. corresponding to the average found for the samples grown using a 35 W B_4C magnetron power, and the scattering length densities were adjusted accordingly. The simulated reflectivity performance is summarized for different supermirrors in Fig. 8.

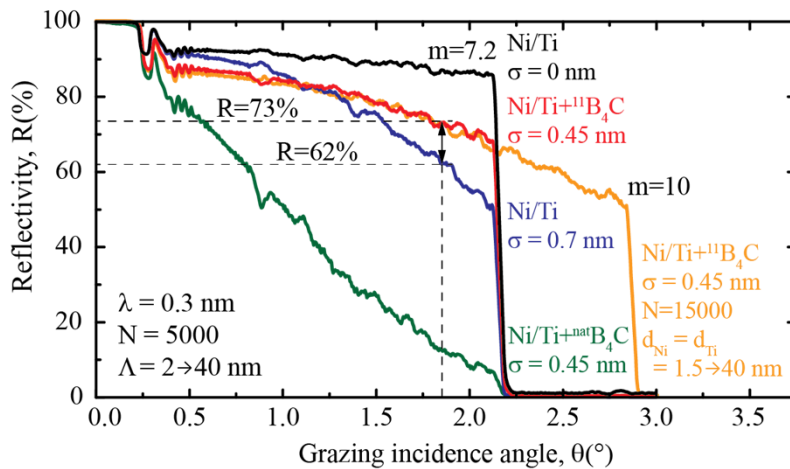


Fig. 8. Reflectivity performance calculated for Ni/Ti and B and C containing Ni/Ti supermirrors: black - ideal Ni/Ti $m = 7.2$ supermirror with theoretical interface width $\sigma = 0.00$ nm; orange - Ni/Ti + $^{11}B_4C$, $\sigma = 0.45$ nm, $m = 10$ supermirror according to the present work, red - Ni/Ti + $^{11}B_4C$, $\sigma = 0.45$ nm according to the present work; blue - Ni/Ti with $\sigma = 0.70$ nm according reported state-of-the-art; green - Ni/Ti + $^{nat}B_4C$, $\sigma = 0.45$ nm according to the present work.

For an ideal supermirror (black curve in Fig. 8) the reflectivity stays above 85% all the way up to the critical angle. The deviation between the ideal calculation and the state-of-the-art reflectivities (blue curve) is solely due to the reported interface width of 0.7 nm. As can be seen, the deviation is increasing for higher grazing incidence angles, corresponding to neutron reflection from thinner layers in the supermirror structure. For thinner layers, the interfaces constitute a larger portion of the structure, and thus any deviations from a perfect interface will have a larger negative influence on the reflectivity at higher angles.

From the simulations it is clear that a Ni/Ti multilayer containing *natural* B and C (green curve) is not suitable as a supermirror. The reason for the low reflectivity is due to the high neutron absorption of the isotope ^{10}B , which constitute 20% of natural B. On the contrary, the ^{11}B isotope has a very low neutron absorption, the imaginary part of the scattering length density is about 6 orders of magnitude lower than for ^{10}B . Thus, if an isotope-enriched $^{11}B_4C$ target material is used for the depositions of a supermirror there are virtually no limitations with respect to absorption (red and orange curves in Fig. 8). Such target materials are readily available, currently at less than twice the cost of a natural B_4C target material.

For low incidence angles, below 1.1° , the simulated reflectivity of the supermirror containing isotope-enriched ^{11}B and C is lower than the one from the state-of-the-art supermirror, despite an interface width of only 0.45 nm. The reason is that at these angles the neutrons are reflected from the thicker layers, which are less sensitive to the interface width, and instead the diluted optical contrast between the layers when using ^{11}B and C is dominating and reduces the reflectivity. However, since the effect of a lower interface width is more important for the reflectivity, the diluted optical contrast is compensated at higher grazing incidence angles, and the reflectivity is higher than state-of-the-art from 1.1° up to the critical angle of the supermirror when using ^{11}B and C.

When considering a neutron waveguide application, it should be realized that an increased supermirror reflectivity leads to a corresponding neutron throughput that increases exponentially with the number of reflections occurring through the waveguide. As an example, neutrons travelling in a 100 m long waveguide of 5 cm width at an incidence angle of 6 times the critical angle of Ni ($m = 6$) will encounter an average of $n = 10$ reflections. Thus, the neutron transmission, using reported state-of-the-art supermirrors with interface width 0.7 nm and a reflectance of $R = 62\%$, will be only $R^n = 0.62^{10} = 0.84\%$.

As a comparison, our results, indicating an improvement in interface width to 0.45 nm using isotope-enriched $^{11}\text{B}_4\text{C}$ -containing Ni/Ti multilayers, yields a reflectance of 73% at $m = 6$, with a corresponding waveguide transmission for neutrons reflected at this specific angle of as much as 4.3%, i.e. an increase by >500%! Thus, a small increase in supermirror reflectivity, by an improved interface quality, has the potential to increase the neutron transmission tremendously.

In addition to an improved reflectivity performance, a reduced interface width will allow even thinner layers to be deposited in the mirror stack and thus higher m-values will be reachable, although at the expense of an increasing number of periods ($N \approx 4m^4$ [40]). The prediction in Fig. 8 indicates that a reflectivity of about 50% could be reached at the critical angle for an $m = 10$ supermirror, which is about the same reflectivity that can be achieved at $m = 7$ today. Thus, not only an increased neutron waveguide transmission is expected, but also neutrons with higher energies will be transmitted, extending the applicability of neutron waveguides to the regime of hot and epithermal neutrons. The general trend during the last decade has been towards larger m-values [41,42], corresponding to thinner and more layers, with prospects of significantly increased neutron waveguide transmissions.

4. Summary

The current limitation in state-of-the-art multilayer neutron mirrors is the manufacturing process to produce layers with smooth and abrupt interfaces. Here a simple growth concept for improved layer morphology control using B and C incorporation in Ni/Ti multilayer mirrors has been explored. By employing co-sputter deposition of B_4C , to amorphize the layers to eliminate nanocrystallites and nano-facets, and a modulated ion assistance during growth, to realize abrupt interfaces and dense layers with smooth top surfaces, interface widths of 0.45 nm was demonstrated. This enables thinner layers to be deposited and predicts largely improved neutron reflectivities by using isotope-enriched $^{11}\text{B}_4\text{C}$, and thus shows very good prospects for long neutron supermirror waveguides with possible m-values as high as 10.

Funding. Stiftelsen för Strategisk Forskning; Vetenskapsrådet.

Acknowledgements. This work was supported by the Swedish Foundation for Strategic Research (SSF) and the Swedish national graduate school in neutron scattering (SwedNess), and the Swedish Research Council (VR). JB acknowledges the Swedish Government Strategic Research Area in Materials Science on Advanced Functional Materials at Linköping University (Faculty Grant SFO Mat LiU No. 2009 00971) for financial support. The authors would like to acknowledge Mauricio Sortica and the support from the Swedish research council VR-RFI (#2017-00646_9) for the Accelerator based ion-technological center, and from the Swedish Foundation for Strategic Research (contract RIF14-0053) for the tandem accelerator laboratory in Uppsala for assistance with Elastic Recoil Detection Analysis.

Disclosures. The authors declare no conflicts of interest.

Data Availability. Data underlying the results presented in this paper are not publicly available at this time but may be obtained from the authors upon reasonable request.

References

1. H. Danared, M. Eshraqi, and M. Jensen, "The ESS Accelerator," in *57th ICFA Advanced Beam Dynamics Workshop on High-Intensity and High-Brightness Hadron Beams* (2016).
2. D. Liu, B. Khaykovich, M.V. Gubarev, J. Lee Robertson, L. Crow, B. D. Ramsey, and D. E. Moncton, "Demonstration of a novel focusing small-angle neutron scattering instrument equipped with axisymmetric mirrors," *Nat. Commun.* **4**(1), 2556 (2013).
3. R. Maruyama, D. Yamazaki, T. Ebisawa, and K. Soyama, "Development of high-reflectivity neutron supermirrors using an ion beam sputtering technique," *Nucl. Instrum. Methods Phys. Res., Sect. A* **600**(1), 68–70 (2009).
4. S. Singh, S. Basu, P. Bhatt, and A. K. Poswal, "Kinetics of alloy formation at the interfaces in a Ni-Ti multilayer: X-ray and neutron reflectometry study," *Phys. Rev. B* **79**(19), 195435 (2009).
5. T. Veres, S. Sajti, L. Cser, S. Bálint, and L. Bottyán, "Roughness replication in neutron supermirrors," *J. Appl. Crystallogr.* **50**(1), 184–191 (2017).
6. M. Ay, C. Schanzer, M. Wolff, and J. Stahn, "New interface solution for Ni/Ti multilayers," *Nucl. Instrum. Methods Phys. Res., Sect. A* **562**(1), 389–392 (2006).
7. M. Senthil Kumar, P. Boni, and M. Horisberger, "Neutron reflectivity and interface roughness in Ni/Ti and FeCoV/TiNx supermirrors," *Nucl. Instrum. Methods Phys. Res., Sect. A* **529**(1-3), 90–93 (2004).
8. A. Biswas, A. Porwal, D. Bhattacharya, C. L. Prajapati, A. Ghosh, M. Nand, C. Nayak, S. Rai, S. N. Jha, M. R. Singh, D. Bhattacharyya, S. Basu, and N. K. Sahoo, "Effect of dry air on interface smoothening in reactive sputter deposited Co/Ti multilayer," *Appl. Surf. Sci.* **416**, 168–177 (2017).
9. K. Soyama, M. Suzuki, Y. Kawabata, T. Ebisawa, and S. Tasaki, "Experimental study on fabrication technique of a Ni/Ti supermirror using the electron beam evaporation system," *J. Nucl. Sci. Technol.* **35**(11), 750–758 (1998).
10. P. Hoghoj, I. Anderson, R. Siebrecht, W. Graf, and K. Ben-Saidane, "Neutron polarizing Fe/Si mirrors at ILL," *Phys. B* **267–268**, 355–359 (1999).
11. M. Hino, T. Oda, M. Kitaguchi, N. L. Yamada, S. Tasaki, and Y. Kawabata, "The ion beam sputtering facility at KURRI: Coatings for advanced neutron optical devices," *Nucl. Instrum. Methods Phys. Res., Sect. A* **797**, 265–270 (2015).
12. M. Gupta, S. M. Amir, A. Gupta, and J. Stahn, "Surfactant mediated growth of Ti/Ni multilayers," *Appl. Phys. Lett.* **98**(10), 101912 (2011).
13. K. Soyama, W. Ishiyama, and K. Murakami, "Enhancement of reflectivity of multilayer neutron mirrors by ion polishing: optimization of the ion beam parameters," *J. Phys. Chem. Solids* **60**(8-9), 1587–1590 (1999).
14. N. Ghafoor, F. Eriksson, A. Aquila, E. Gullikson, F. Schäfers, G. Greczynski, and J. Birch, "Impact of B₄C co-sputtering on structure and optical performance of Cr/Sc multilayer X-ray mirrors," *Opt. Express* **25**(15), 18274–18287 (2017).
15. F. Mezei and P. A. Dagleish, "Corrigendum and first experimental evidence on neutron supermirrors," *Commun. Phys.* **2**, 41–43 (1977).
16. A. Paul, A. Teichert, T. Krist, and R. Steitz, "Substrate-stress-induced magnetic and nonmagnetic structural correlations in Fe/Si multilayers," *J. Appl. Crystallogr.* **48**(4), 1023–1033 (2015).
17. Z. Zhang, Z.-S. Wang, J.-T. Zhu, F.-L. Wang, Y.-R. Wu, S.-J. Qin, and L.-Y. Chen, "Design and Fabrication of Ni/Ti Multilayer for Neutron Supermirror," *Chin. Phys. Lett.* **23**(10), 2678–2680 (2006).
18. S.-J. Cho, Th. Krist, and F. Mezei, "Determination of interface growth with atomic resolution in FeCo–Si multilayers," *Thin Solid Films* **434**(1-2), 136–144 (2003).
19. J. L. Schroeder, W. Thomson, B. Howard, N. Schell, L. A. Naslund, L. Rogstrom, M. P. Johansson-Joesaar, N. Ghafoor, M. Oden, E. Nothnagel, A. Shepard, J. Greer, and J. Birch, "Industry-relevant magnetron sputtering and cathodic arc ultra-high vacuum deposition system for in situ x-ray diffraction studies of thin film growth using high energy synchrotron radiation," *Rev. Sci. Instrum.* **86**(9), 095113 (2015).
20. F. Eriksson, N. Ghafoor, F. Schäfers, E. M. Gullikson, and J. Birch, "Interface engineering of short-period Ni/V multilayer X-ray mirrors," *Thin Solid Films* **500**(1-2), 84–95 (2006).
21. F. Eriksson, F. Schäfers, E. M. Gullikson, S. Aouadi, N. Ghafoor, S. Rohde, L. Hultman, and J. Birch, "Atomic scale interface engineering by modulated ion-assisted deposition applied to soft x-ray multilayer optics," *Appl. Opt.* **47**(23), 4196–4204 (2008).
22. H. J. Whitlow, G. Possnert, and C. S. Petersson, "Quantitative mass and energy dispersive elastic recoil spectrometry: Resolution and efficiency considerations," *Nucl. Instrum. Methods Phys. Res., Sect. B* **27**(3), 448–457 (1987).
23. J. Jensen, D. Martin, A. Surpi, and T. Kubart, "ERD analysis and modification of TiO₂ thin films with heavy ions," *Nucl. Instrum. Methods Phys. Res., Sect. B* **268**(11-12), 1893–1898 (2010).
24. K. Arstila, J. Julin, M. Laitinen, J. Aalto, T. Konu, S. Kärkkäinen, S. Rahkonen, M. Raunio, J. Itkonen, J.-P. Santanen, T. Tuovinen, and T. Sajavaara, "Potku – New analysis software for heavy ion elastic recoil detection analysis," *Nucl. Instrum. Methods Phys. Res., Sect. B* **331**, 34–41 (2014).
25. G. Greczynski and L. Hultman, "C 1s peak of adventitious carbon aligns to the vacuum level: dire consequences for material's bonding assignment by photoelectron spectroscopy," *ChemPhysChem* **18**(12), 1507–1512 (2017).

26. N. Fairly, *Surface Analysis by Auger and X-ray Photoelectron Spectroscopy*, D. B. J. Grant, ed., (IM Publications, 2003), 397–398.
27. D. L. Windt, “IMD—Software for modeling the optical properties of multilayer films,” *Comput. Phys.* **12**(4), 360 (1998).
28. H. Aboulfadl, F. Seifried, M. Stüber, and F. Mücklich, “Interdiffusion in as-deposited Ni/Ti multilayer thin films analyzed by atom probe tomography,” *Mater. Lett.* **236**, 92–95 (2019).
29. O. Elsenhans, P. Böni, H. P. Friedli, H. Grimmer, P. Buffat, K. Leifer, J. Söchtig, and I. S. Anderson, “Development of Ni/Ti multilayer supermirrors for neutron optics,” *Thin Solid Films* **246**(1-2), 110–119 (1994).
30. S. Tanuma, C. J. Powell, and D. Penn, “Calculations of electron inelastic mean free paths. IX. Data for 41 elemental solids over the 50 eV to 30 keV range,” *Surf. Interface Anal.* **43**(3), 689–713 (2011).
31. F. R. De Boer, R. Boom, W. C. Mattens, A. R. Miedema, and A. K. Niessen, *Cohesion in Metals* (North-Holland, 1988).
32. S. Berg and I. Katardjiev, “Resputtering effects during ion beam assisted deposition and the sputter yield amplification effect,” *Surf. Coat. Technol.* **84**(1-3), 353–362 (1996).
33. G. Greczynski and L. Hultman, “Towards reliable X-ray photoelectron spectroscopy: Sputter-damage effects in transition metal borides, carbides, nitrides, and oxides,” *Appl. Surf. Sci.* **542**, 148599 (2021).
34. E. S. Domalski and G. T. Armstrong, “The Heat of Formation of Boron Carbide,” *J. Res. Natl. Bur. Stand., Sect. A* **72A**(2), 133–139 (1968).
35. P. Bhatt, R. Prakash, S. M. Chaudhari, V. R. Reddy, and D. M. Phase, “Investigation of Ti layer thickness dependent structural, magnetic, and photoemission study of nanometer range Ti/Ni multilayer structures,” *J. Nanosci. Nanotechnol.* **7**(6), 2081–2086 (2007).
36. J. B. Hayter and H. A. Mook, “Discrete thin-film multilayer design for X-ray and neutron supermirrors,” *J. Appl. Crystallogr.* **22**(1), 35–41 (1989).
37. I. Carron and V. Ignatovich, “Algorithm for preparation of multilayer systems with high critical angle of total reflection,” *Phys. Rev. A* **67**(4), 043610 (2003).
38. N. K. Pleshakov, “Algorithm for the real-structure design of neutron supermirrors,” *Nucl. Instrum. Methods Phys. Res., Sect. A* **524**(1-3), 273–286 (2004).
39. S. Masalovich, “Analysis and design of multilayer structures for neutron monochromators and supermirrors,” *Nucl. Instrum. Methods Phys. Res., Sect. A* **722**, 71–81 (2013).
40. P. Böni, “Supermirror-based beam devices,” *Phys. B* **234-236**, 1038–1043 (1997).
41. M. Hino, H. Hayashida, M. Kitaguchi, Y. Kawabata, M. Takeda, R. Maruyama, T. Ebisawa, N. Torikai, T. Kume, and S. Tasaki, “Development of large-m polarizing neutron supermirror fabricated by using ion beam sputtering instrument at KURRI,” *Phys. B* **385-386**, 1187–1189 (2006).
42. R. Maruyama, D. Yamazaki, T. Ebisawa, M. Hino, and K. Soyama, “Development of neutron supermirrors with large critical angle,” *Thin Solid Films* **515**(14), 5704–5706 (2007).